Supporting Information

Electrodeposited Zeolitic Imidazolate Framework-8 Modified Zinc Anode Supported Over Porous Copper Structure for Rechargeable Aqueous Zinc-Ion Batteries

Abhas Anand, Anil Verma, and Suddhasatwa Basu*

Department of Chemical Engineering, Indian Institute of Technology Delhi, New Delhi, 110016, India.

**Corresponding Author:* sbasu@iitd.ac.in

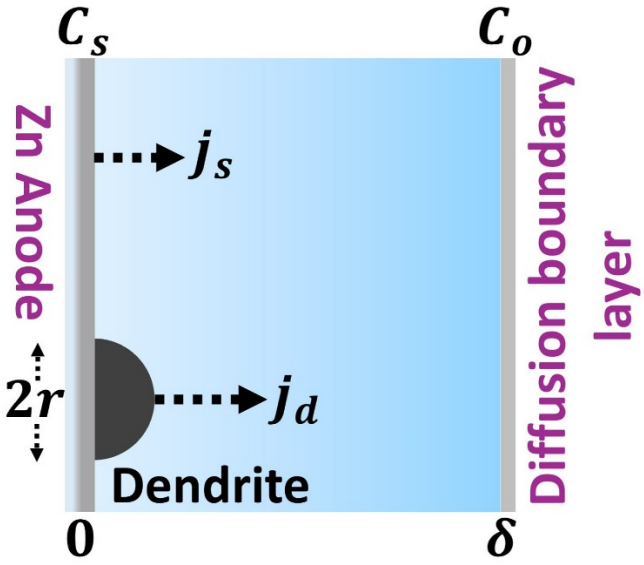

Figure S1. Schematic diagram illustrating the model geometry of Zn-based anode.

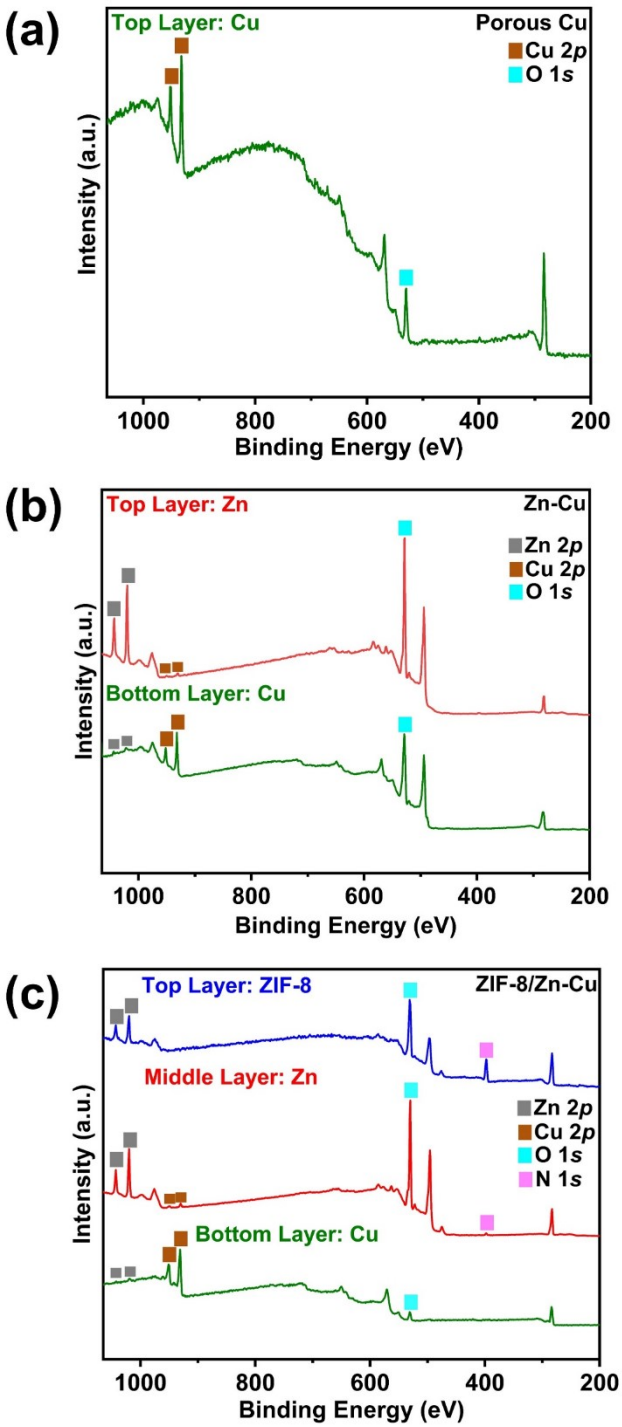

Figure S2. Layer-by-layer XPS survey spectra of (a) Porous Cu (b) Zn-Cu (c) ZIF-8/Zn-Cu.

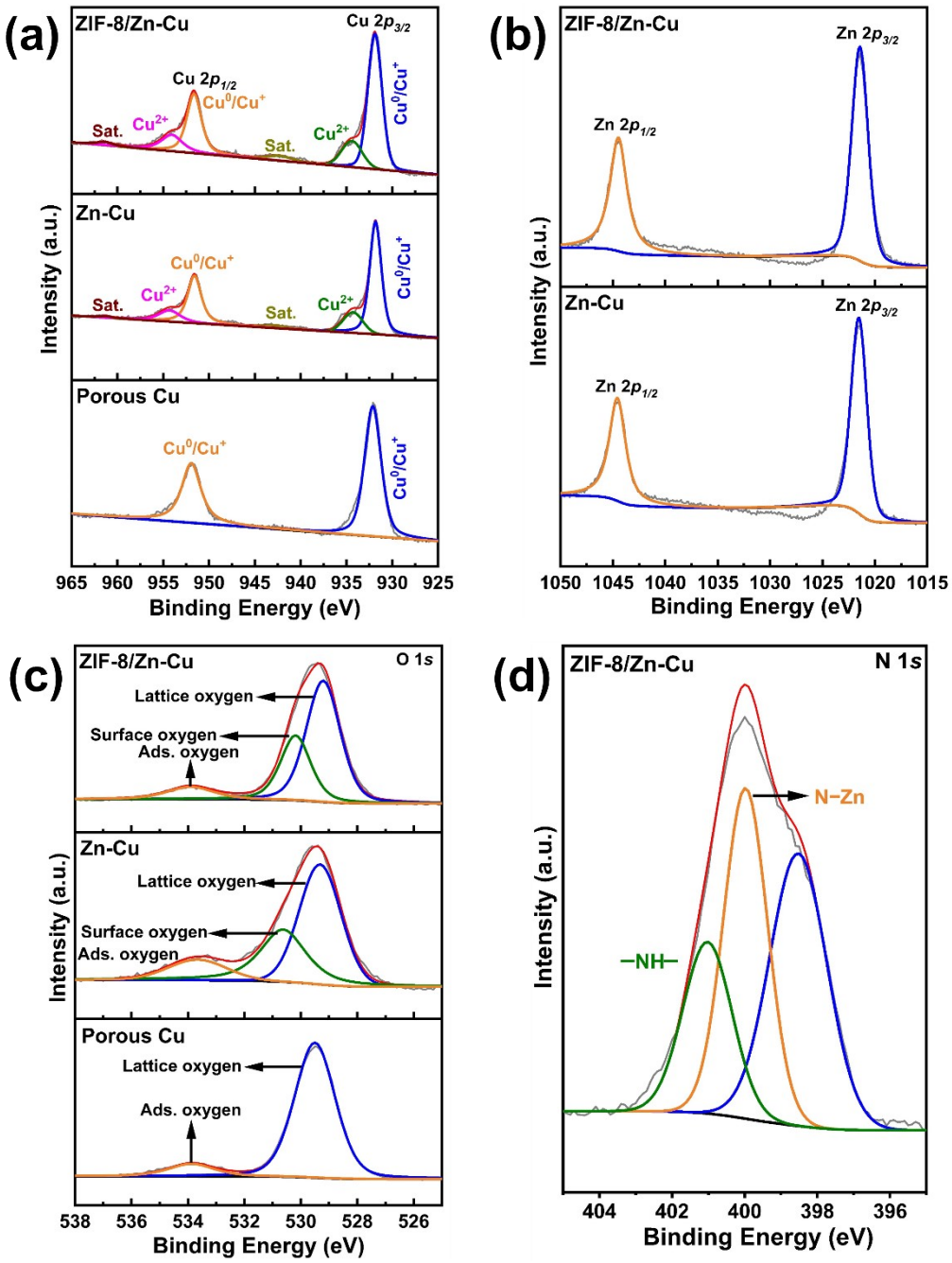

Figure S3. High-resolution XPS spectra of (a) Cu 2*p* for porous Cu, Zn-Cu, and ZIF-8/Zn-Cu (b) Zn 2*p* for Zn-Cu and ZIF-8/Zn-Cu (c) O 1*s* for porous Cu, Zn-Cu, and ZIF-8/Zn-Cu (d) N 1*s* for ZIF-8/Zn-Cu.

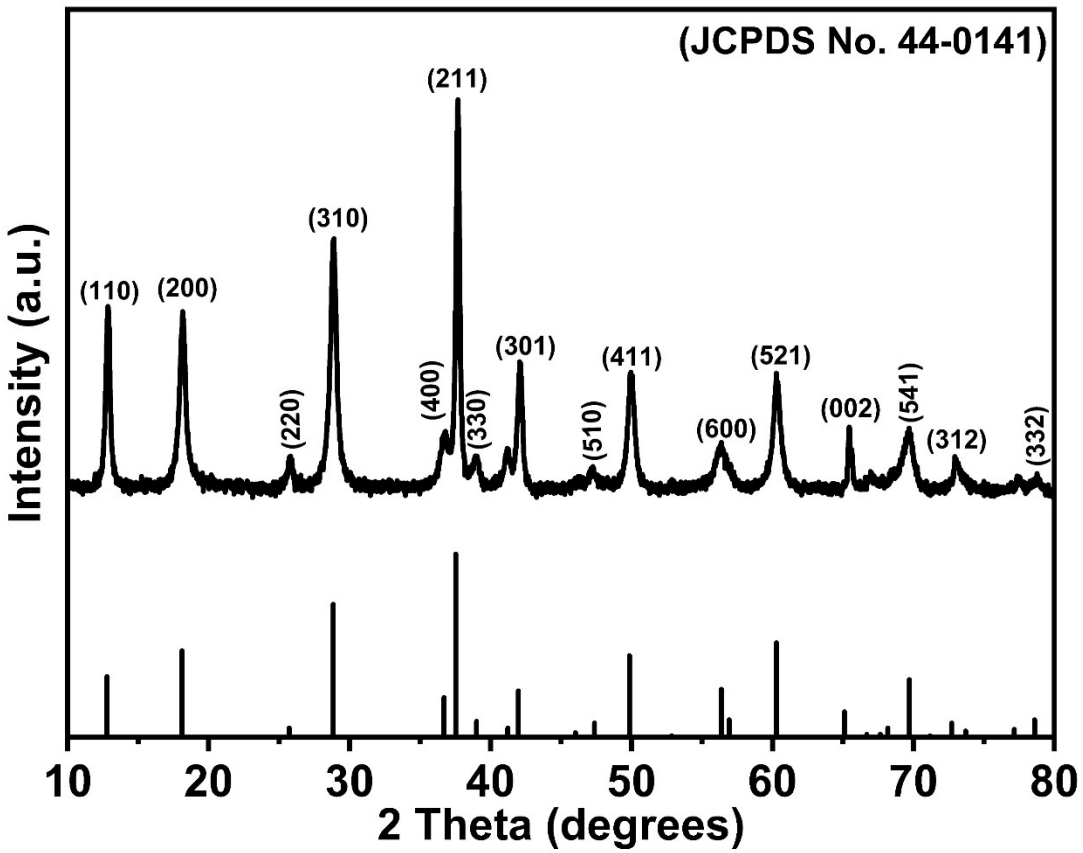

Figure S4. XRD pattern of α-MnO_2.

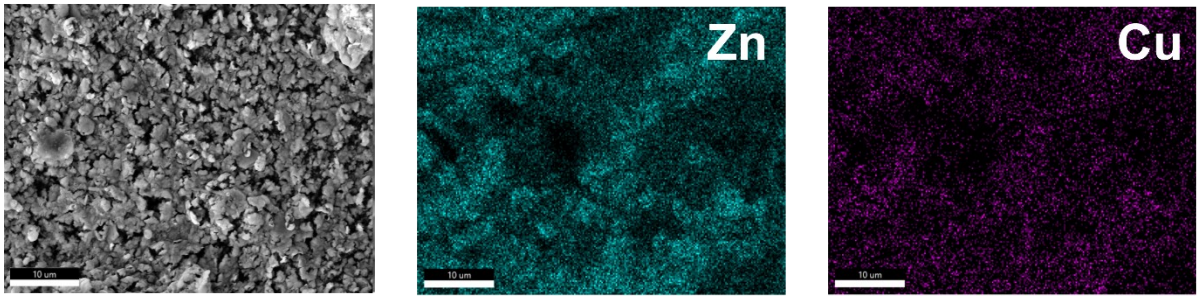

Figure S5. EDX mapping of fabricated Zn-Cu electrode.

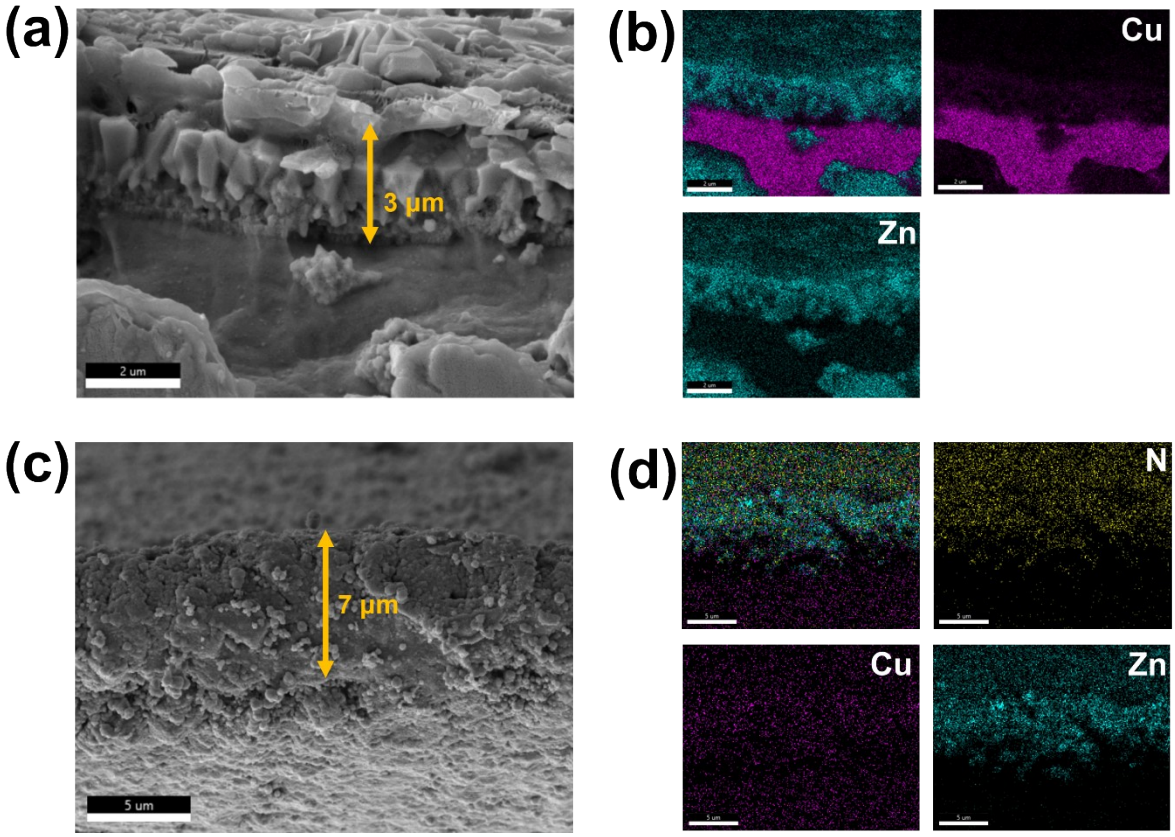

Figure S6. Cross-sectional FESEM images (a, c) and EDX mapping (b, d) of Zn-Cu and ZIF-8/Zn-Cu electrodes.

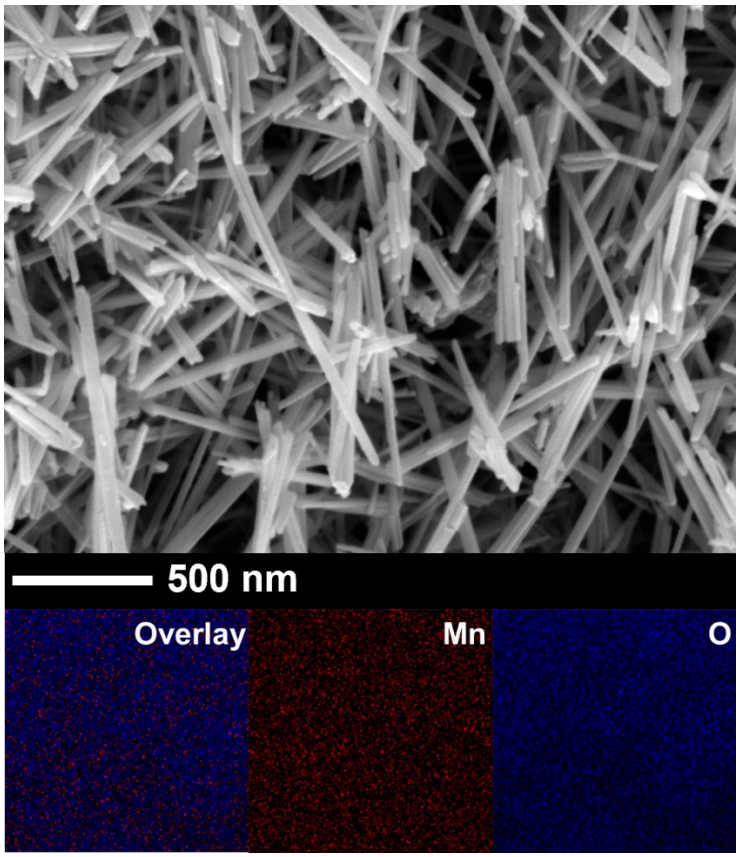

Figure S7. FESEM image and EDX mapping of synthesized α-MnO_2.

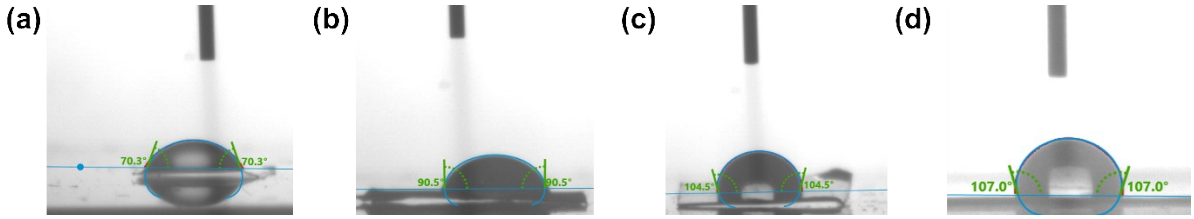

Figure S8. Contact angle of (a) Pristine Zn (b) Zn-Cu (c) ZIF-8/Zn-Cu (d) ZIF-8.

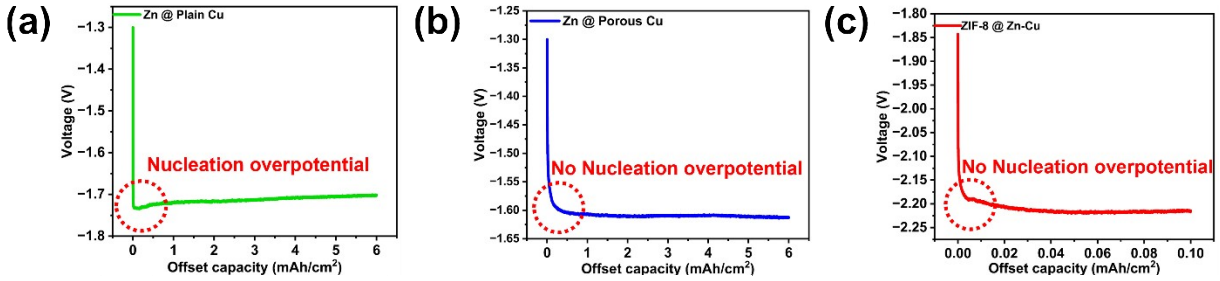

Figure S9. Electrodeposition voltage profile of (a) Zn @ Pristine Cu (b) Zn @ Porous Cu (c) ZIF-8 @ Zn-Cu.

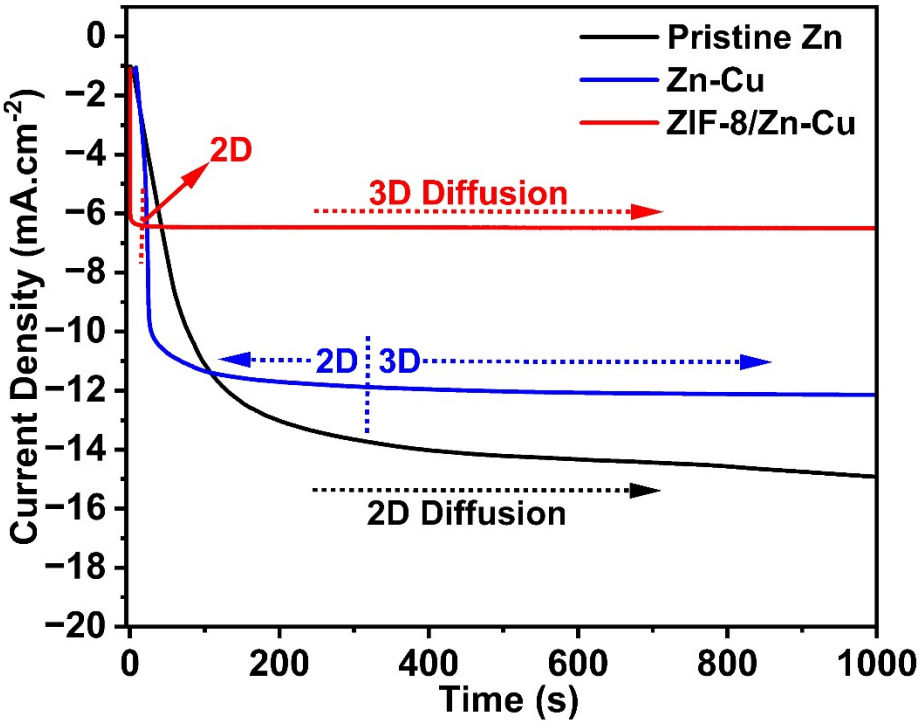

Figure S10. Chronoamperometry plot of pristine Zn, Zn-Cu, and ZIF-8/Zn-Cu electrodes at an applied overpotential of -120 mV vs. OCV.

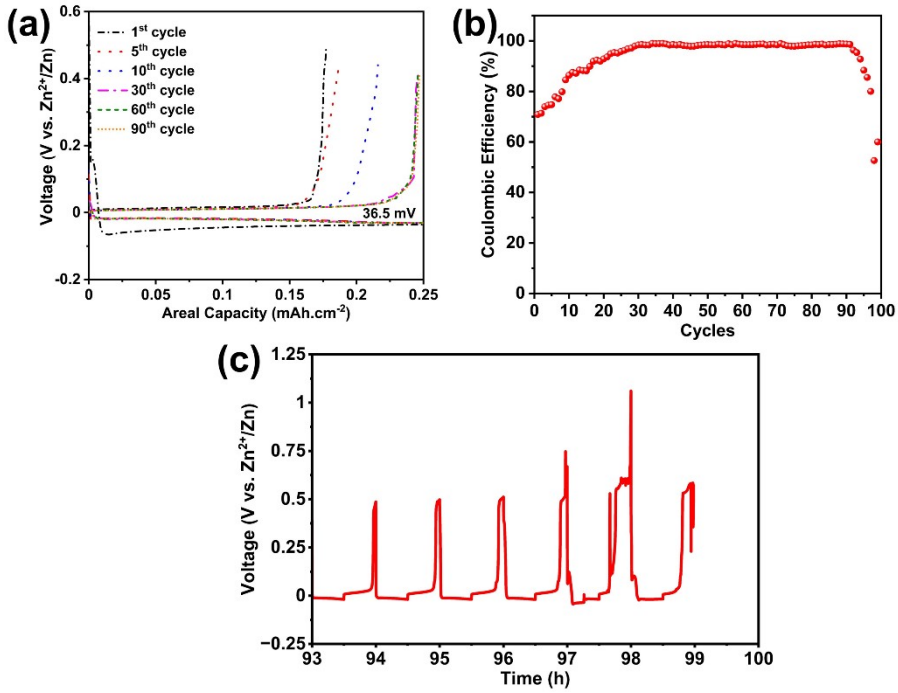

Figure S11. Zn//Cu asymmetric cell test at 0.5 mA.cm^{-2} in 2 M $ZnSO_4$ electrolyte under 1 hour cycling intervals. (a) Discharge/charge voltage profiles of Zn plating/stripping (b) Variation of Coulombic efficiency over cycling (c) Enlarged voltage profiles between 93 and 99 hours of cycling period.

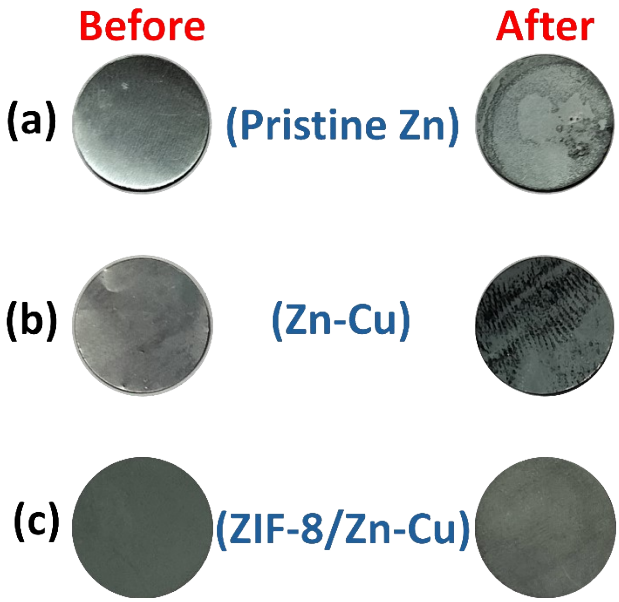

Figure S12. Digital images of the pristine Zn, Zn-Cu, and ZIF-8/Zn-Cu anodes before and after symmetrical cell testing at a current density of 0.5 $mA.cm^{-2}$.

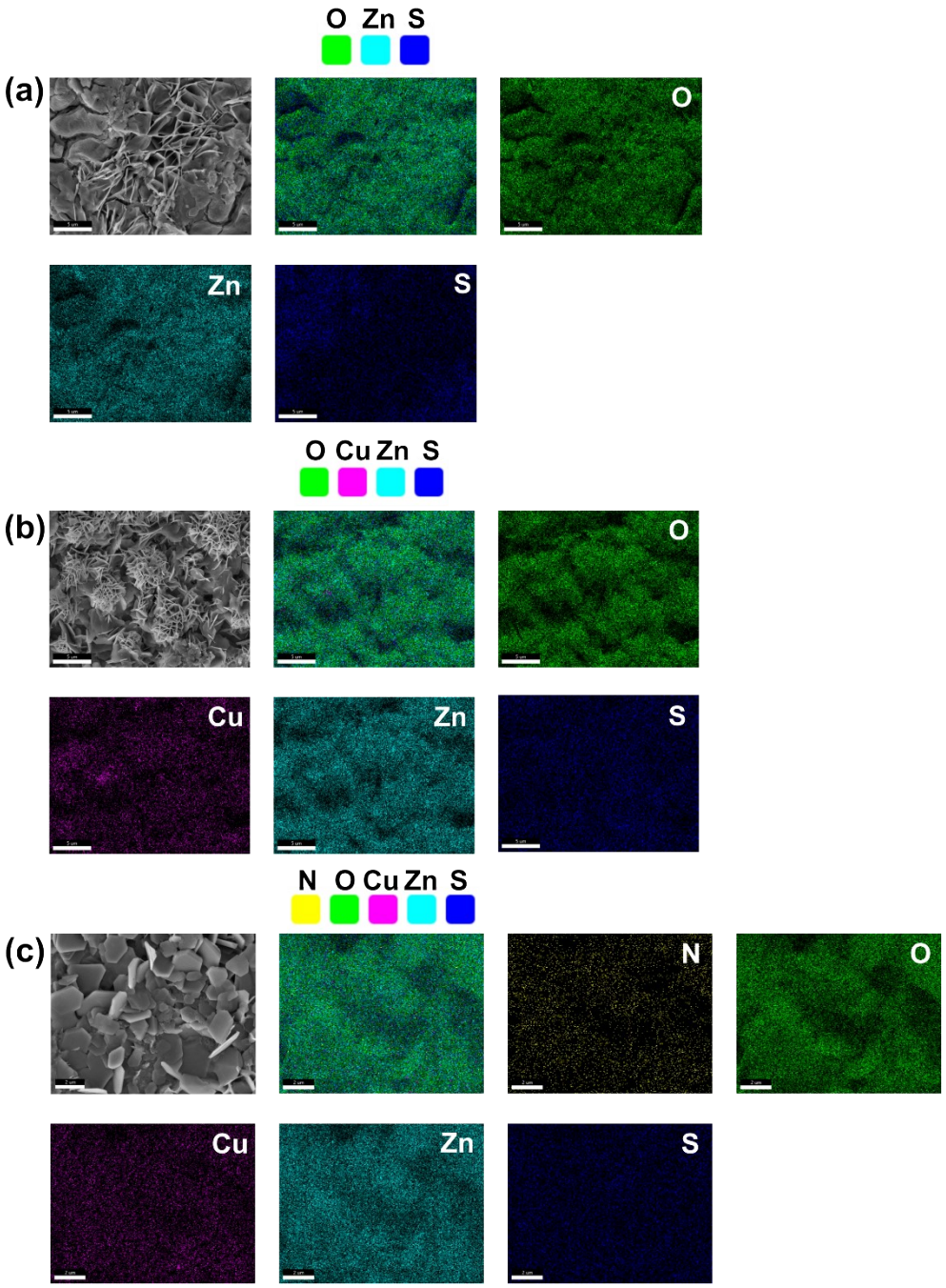

Figure S13. EDX mapping of the post-cycled anodes at 0.5 mA.cm^{-2} from (b, c) Zn//Zn (d, e) Zn-Cu//Zn-Cu (f, g) ZIF-8/Zn-Cu//ZIF-8/Zn-Cu.

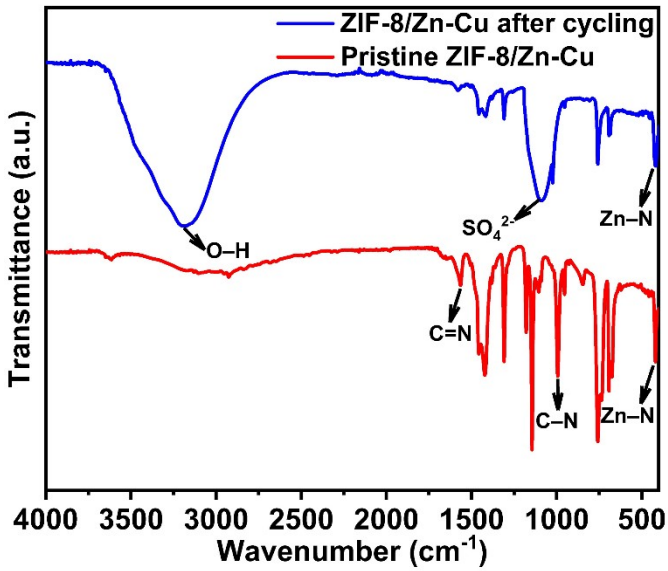

Figure S14. FTIR spectra of ZIF-8/Zn-Cu in pristine electrode and after 1000 cycles of symmetric cell testing.

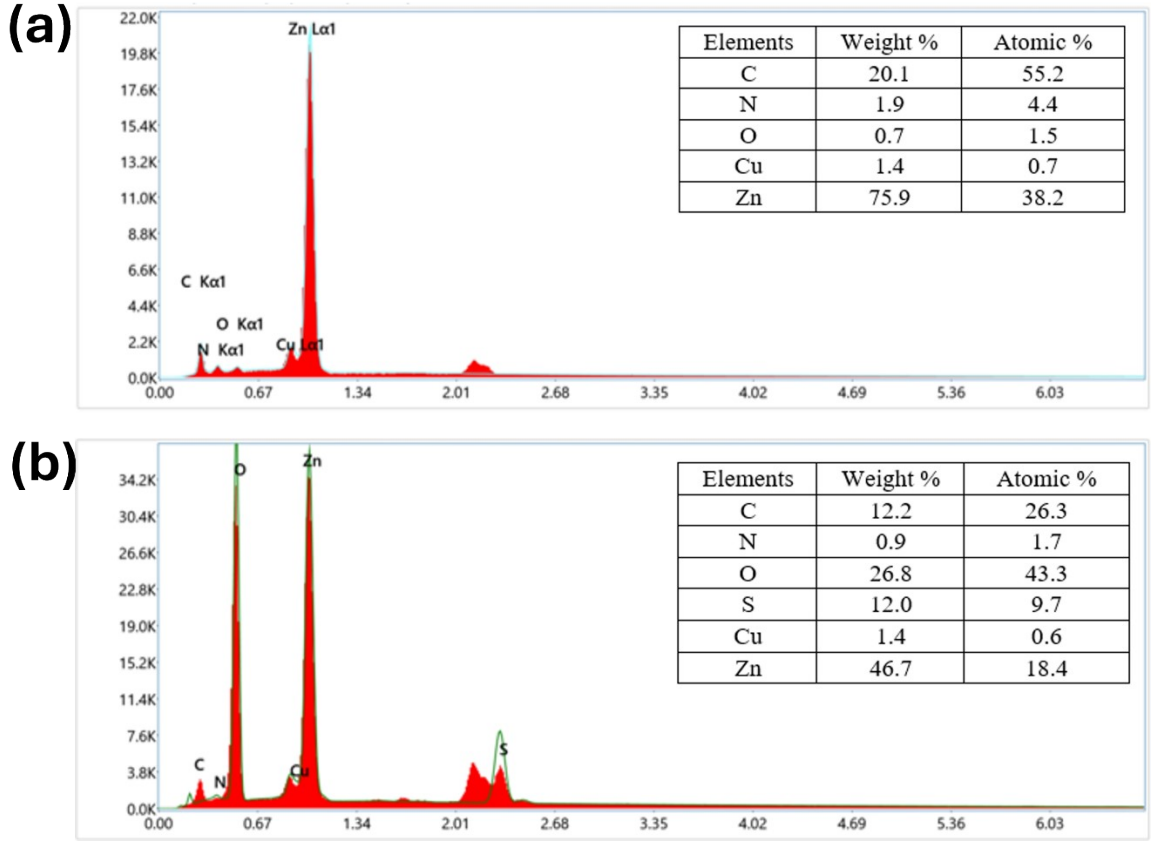

Elements	Weight %	Atomic %
C	20.1	55.2
N	1.9	4.4
O	0.7	1.5
Cu	1.4	0.7
Zn	75.9	38.2

Elements	Weight %	Atomic %
C	12.2	26.3
N	0.9	1.7
O	26.8	43.3
S	12.0	9.7
Cu	1.4	0.6
Zn	46.7	18.4

Figure S15. EDX spectra of the ZIF-8/Zn-Cu electrode in the (a) fresh electrode and (b) electrode after symmetric cell testing.

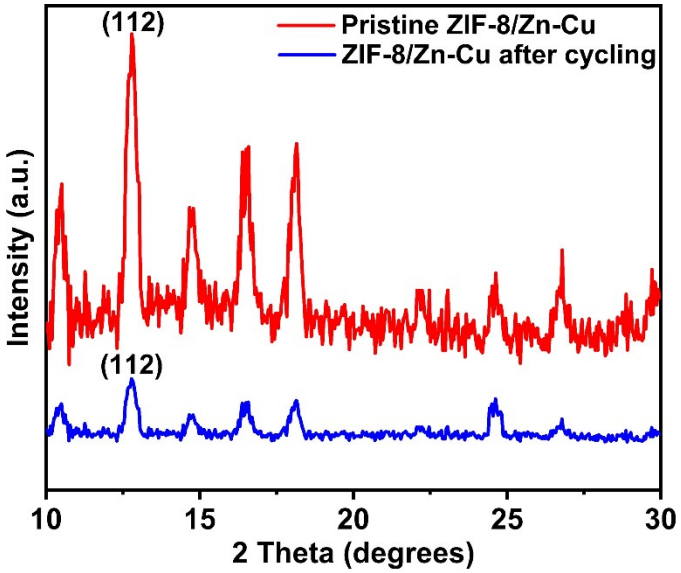

Figure S16. Magnified XRD patterns of ZIF-8/Zn-Cu in pristine electrode and after 1000 cycles of symmetric cell testing.

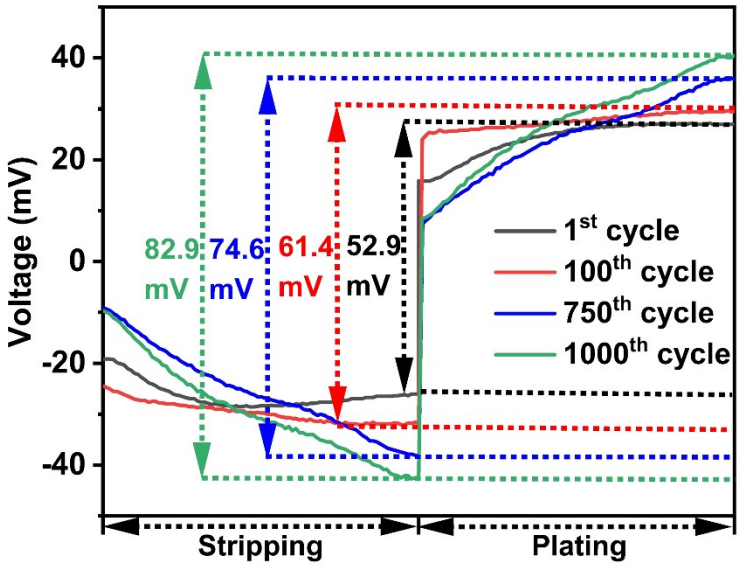

Figure S17. Comparison of voltage profiles of the ZIF-8/Zn-Cu//ZIF-8/Zn-Cu symmetric cell at different cycles and at 0.5 mA.cm^{-2} with 1 hour cycling intervals.

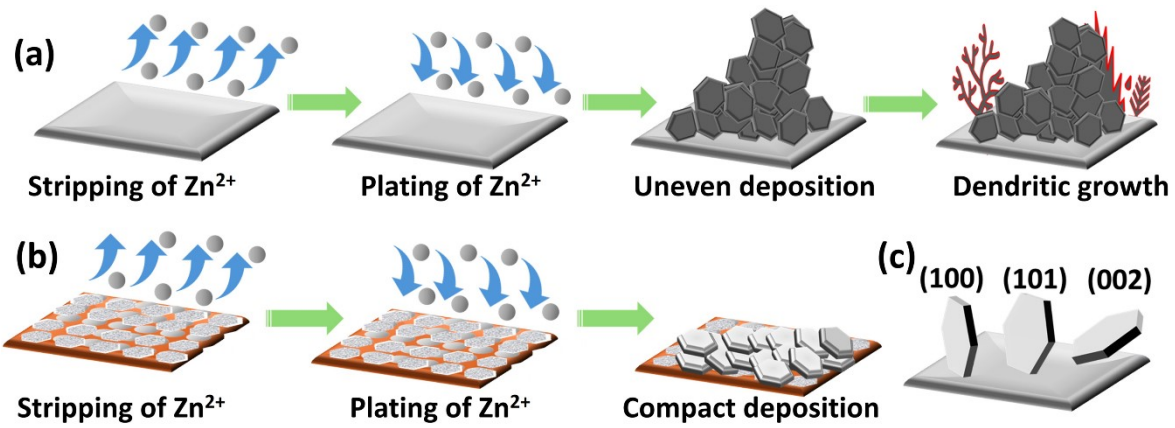

Figure S18. Schematic of Zn deposition behaviour for (a) pristine Zn (b) ZIF-8/Zn-Cu. (c) Schematic representation of the different crystal facets in metallic Zn.

S1. Description for the calculation of D, a, b, and δ

To determine the constants (a and b) associated with the concentration-dependent diffusion coefficient, the D values at two different bulk concentrations of Zn^{2+} were required. Therefore, 2 M and 3 M $ZnSO_4$ electrolyte solutions were used, and the diffusion coefficients of Zn^{2+} $\left((D)_{2M}\ and\ (D)_{3M}\right)$ were calculated using Equations S1 and S2, which are based on the Levich equation using RDE measurements (Figures S19 and S20 in SI). The RDE polarization experiments for the Zn, Zn-Cu, and ZIF-8/Zn-Cu electrodes were carried out in 2 M and 3 M $ZnSO_4$ electrolyte solutions at rotation speeds ranging from 300 to 1500 rpm. A potential scan rate of 10 $mV.s^{-1}$ was applied within the voltage range of -0.96 to -0.9 V (vs. Ag/AgCl). An increase in $ZnSO_4$ concentration from 2 M to 3 M led to a rise in disk current for all three electrode configurations at all rotation speeds, as shown in Figures S19a-c and S20a-c in SI. For all electrodes and electrolyte concentrations, measurable disk currents appeared above -0.95 V (vs. Ag/AgCl), followed by well-defined diffusion-limited current plateaus beyond -0.92 V (vs. Ag/AgCl). The i_L values were taken at -0.9 V (vs. Ag/AgCl) from the polarization curves and

plotted against $\omega^{0.5}$ in accordance with the Levich equation, as shown in Figures S19d-f and S20d-f in SI, to determine L_m. The resulting plots exhibited good linearity, consistent with the theoretical Levich behavior expected for diffusion-controlled processes, with correlation coefficients (R^2) close to unity for both 2 M and 3 M $ZnSO_4$ solutions and all electrode systems. The calculated L_m values for the Zn, Zn-Cu, and ZIF-8/Zn-Cu electrodes were then used to determine the corresponding D values of Zn^{2+} ions in 2 M and 3 M $ZnSO_4$ electrolytes. The D values were found to be on the order of 10^{-13} $m^2.s^{-1}$ for all electrode systems. A slight decrease in the D values was observed with increasing $ZnSO_4$ concentration from 2 M to 3 M, while the overall order of magnitude remained unchanged, as summarized in Table S2.

Equations S3 and S4 were used to calculate the constants (a and b) associated with the concentration-dependent diffusion coefficient. The obtained values of a were 5.54×10^{-13} $m^2.s^{-1}$, 5.02×10^{-13} $m^2.s^{-1}$, and 5.16×10^{-13} $m^2.s^{-1}$ for the pristine Zn, Zn-Cu, and ZIF-8/Zn-Cu electrodes, respectively. Correspondingly, the values of b were 0.000239 $m^3.mol^{-1}$, 0.000213 $m^3.mol^{-1}$, and 0.000257 $m^3.mol^{-1}$ for the respective electrode systems. Moreover, the δ values for all three anode configurations were determined using the Nernst diffusion layer thickness model. A θ value of 0.5 hours was selected for the δ calculation using Equation S5. This selection was based on the experimental setup, where galvanostatic plating/stripping tests were performed in symmetrical cells with each cycle lasting 1 hour-comprising 0.5 hours for plating and 0.5 hours for stripping (Figure 5a). The calculated δ for the pristine Zn, Zn-Cu, and ZIF-8/Zn-Cu electrodes were 44.03×10^{-6} m, 43.06×10^{-6} m, and 41.79×10^{-6} m, respectively.

$$i_L = \left(0.62nFA_g CD^{\frac{2}{3}} \nu^{-\frac{1}{6}}\right)\omega^{\frac{1}{2}} \tag{S1}$$

$$D = \left(\frac{L_m}{0.62nFA_g C\nu^{-\frac{1}{6}}}\right)^{\frac{3}{2}} \tag{S2}$$

$$(D)_{2M} = ae^{-b(C)_{2M}} \tag{S3}$$

$$(D)_{3M} = ae^{-b(C)_{3M}} \tag{S4}$$

$$\delta = \sqrt{\pi(D)_{2M}\theta} \tag{S5}$$

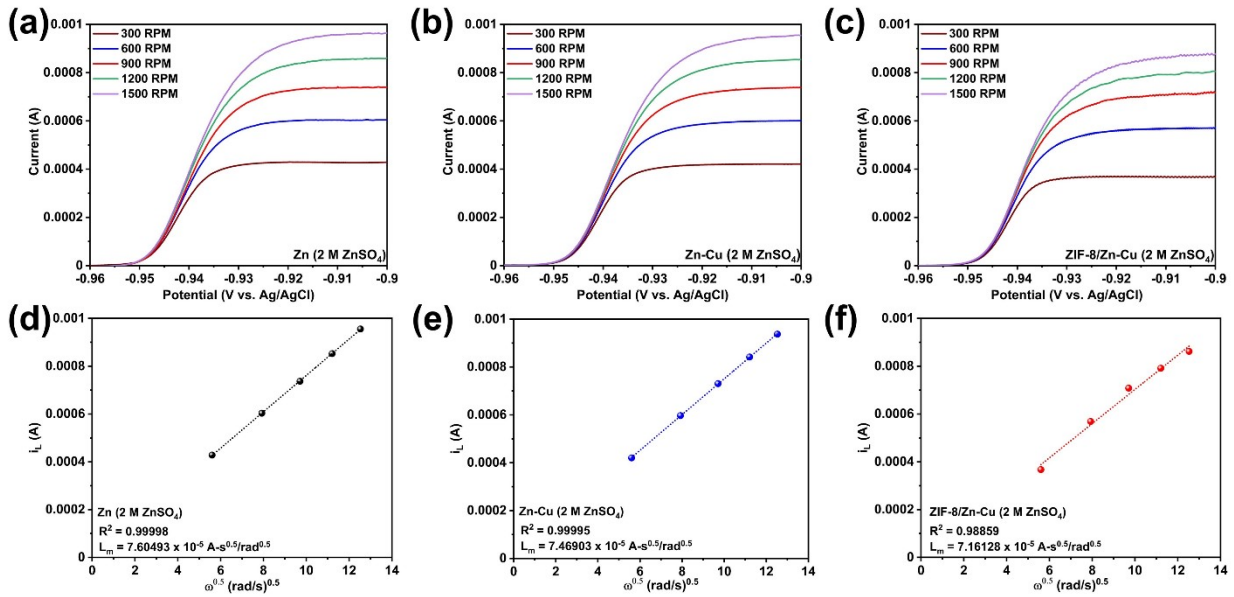

Figure S19. LSV polarisation curves at different rotation speeds in 2 M $ZnSO_4$ for (a) Zn (b) Zn-Cu (c) ZIF-8/Zn-Cu; corresponding Levich plots at -0.9 V (vs. Ag/AgCl) for (d) Zn (e) Zn-Cu (f) ZIF-8/Zn-Cu.

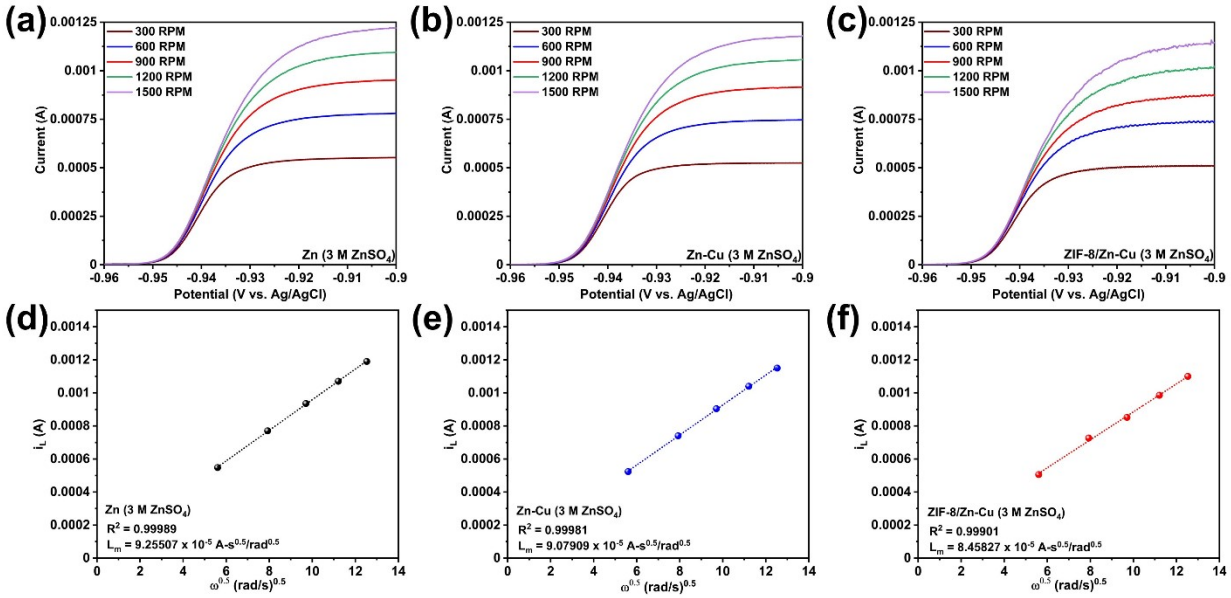

Figure S20. LSV polarisation curves at different rotation speeds in 3 M $ZnSO_4$ for (a) Zn (b) Zn-Cu (c) ZIF-8/Zn-Cu; corresponding Levich plots at -0.9 V (vs. Ag/AgCl) for (d) Zn (e) Zn-Cu (f) ZIF-8/Zn-Cu.

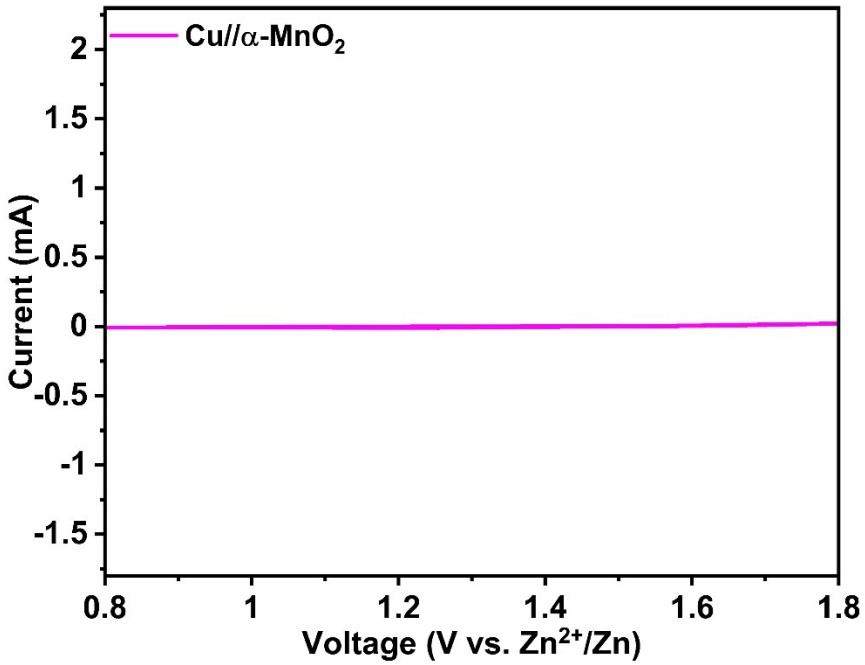

Figure S21. CV curve of Cu//α-MnO_2 at 0.5 mV.sec^{-1}.

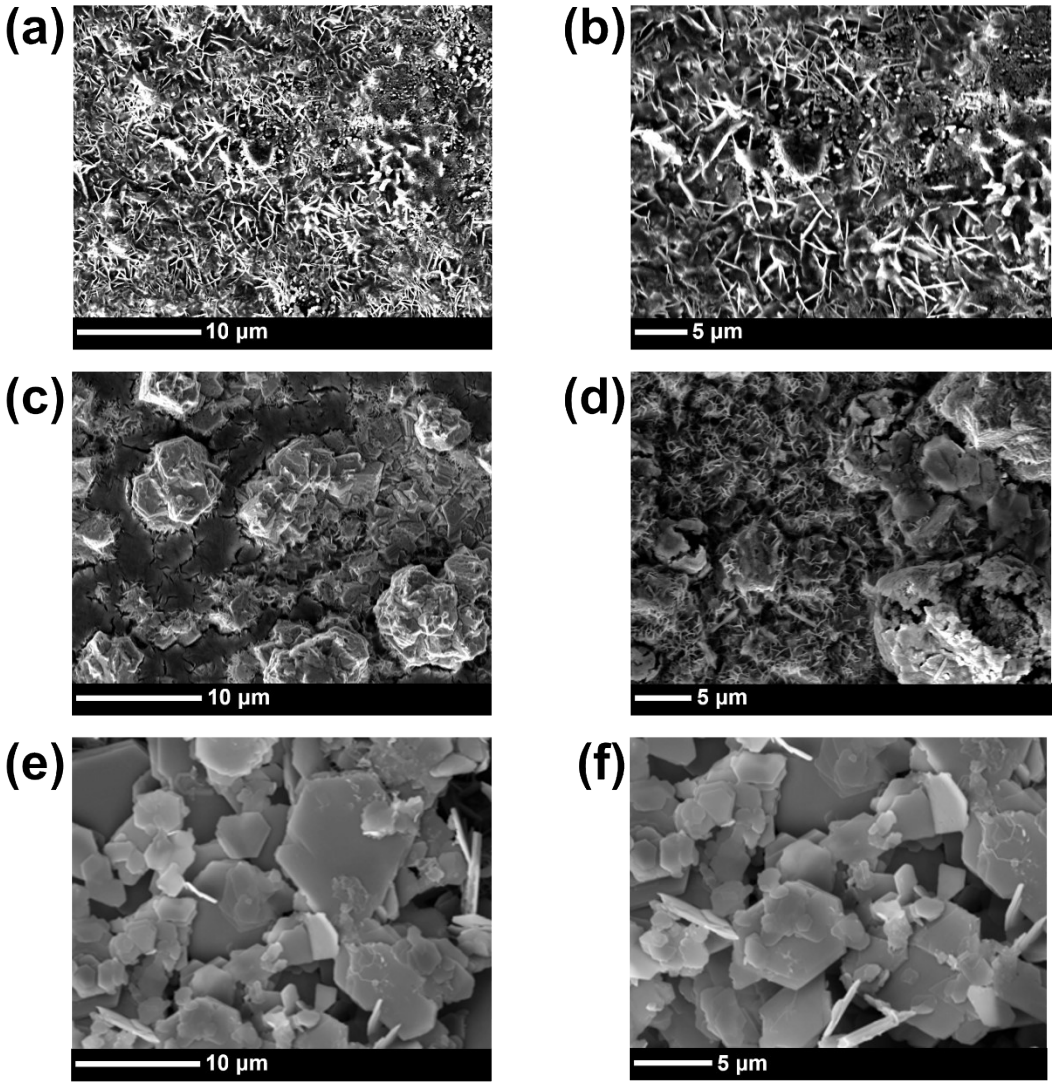

Figure S22. FESEM images of the post-cycled anodes at 0.4 C from (a, b) Zn//α-MnO_2 (c, d) Zn-Cu//α-MnO_2 (e, f) ZIF-8/Zn-Cu//α-MnO_2.

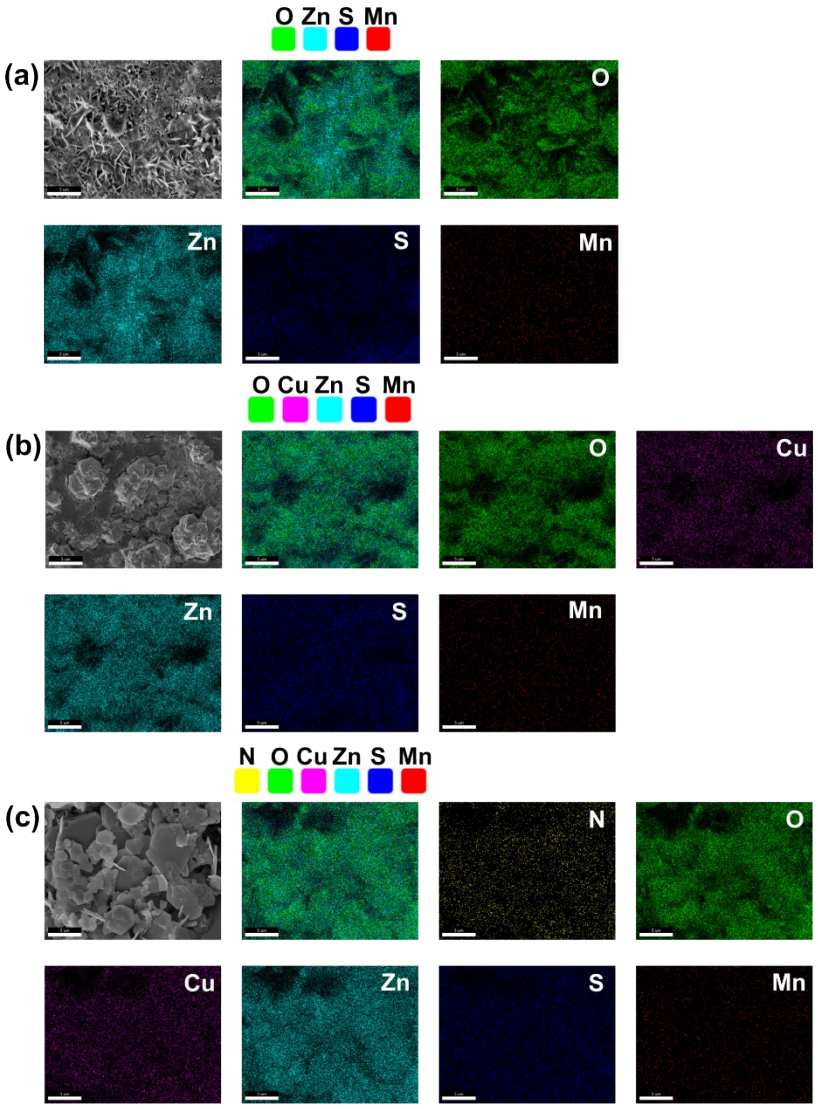

Figure S23. EDX mapping of the post-cycled anodes at 0.4 C from (a, b) Zn//α-MnO_2 (c, d) Zn-Cu//α-MnO_2 (e, f) ZIF-8/Zn-Cu//α-MnO_2.

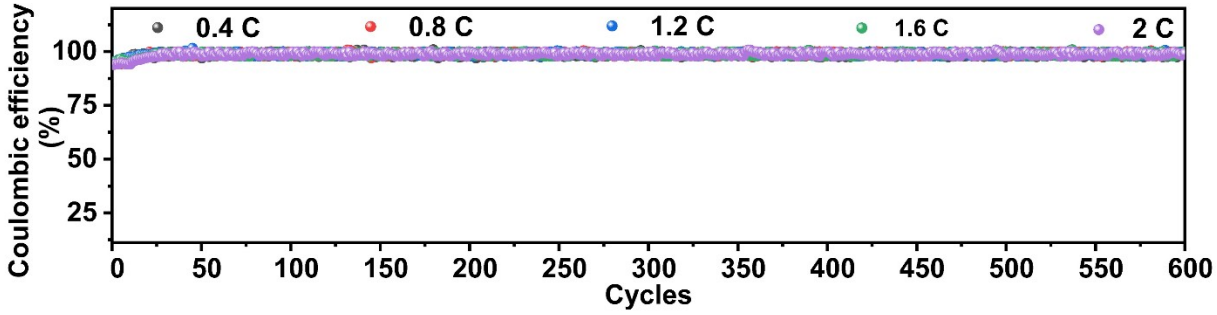

Figure S24. Coulombic efficiency of ZIF-8/Zn-Cu//α-MnO_2 at varied C-rates (0.4 C to 2 C).

Table S1. Constant parameters used in mathematical modelling of Zn-based anodes

Parameters	Zn	Zn-Cu	ZIF-8/Zn-Cu	References
R	8.314 J/mol-K	8.314 J/mol-K	8.314 J/mol-K	-
T	298 K	298 K	298 K	-
A	1.1304 × 10^{-4} m^2	1.1304 × 10^{-4} m^2	1.1304 × 10^{-4} m^2	Experimental
A_g	0.07065 × 10^{-4} m^2	0.07065 × 10^{-4} m^2	0.07065 × 10^{-4} m^2	Experimental
n	2	2	2	-
z_+	2	2	2	-
F	96500 C.mol^{-1}	96500 C.mol^{-1}	96500 C.mol^{-1}	-
C_o	2000 mol.m^{-3}	2000 mol.m^{-3}	2000 mol.m^{-3}	Experimental
j_s	0.5 mA.cm^{-2}	0.5 mA.cm^{-2}	0.5 mA.cm^{-2}	Experimental
α	0.5	0.5	0.5	[1]
M_w	65.38 g.mol^{-1}	65.38 g.mol^{-1}	65.38 g.mol^{-1}	-
ρ_w	7140 kg.m^{-3}	7140 kg.m^{-3}	7140 kg.m^{-3}	-
γ	0.5 J.m^{-2}	0.5 J.m^{-2}	0.5 J.m^{-2}	[1]
κ	0.29 S.m^{-1}	0.29 S.m^{-1}	0.29 S.m^{-1}	[2]

Table S2. Calculated parameters from experimental data and numerical calculations in the mathematical modelling of Zn-based anodes

Parameters	Zn	Zn-Cu	ZIF-8/Zn-Cu
μ_{2M}	0.0021 Pa-s	0.0021 Pa-s	0.0021 Pa-s
μ_{3M}	0.0035 Pa-s	0.0035 Pa-s	0.0035 Pa-s
ρ_{2M}	1323 kg.m^{-3}	1323 kg.m^{-3}	1323 kg.m^{-3}
ρ_{3M}	1484 kg.m^{-3}	1484 kg.m^{-3}	1484 kg.m^{-3}
ν_{2M}	1.5873 × 10^{-6} m^2/s	1.5873 × 10^{-6} m^2/s	1.5873 × 10^{-6} m^2/s
ν_{3M}	2.3585 × 10^{-6} m^2/s	2.3585 × 10^{-6} m^2/s	2.3585 × 10^{-6} m^2/s
i_o	2.748 × 10^{-6} A	6.958 × 10^{-6} A	9.529 × 10^{-6} A
i_{ss}	0.81 × 10^{-6} A	3.069 × 10^{-6} A	6.331 × 10^{-6} A
$\left(R_{o_{CT}}\right)_{2M}$	503.6 Ω	440.7 Ω	432.5 Ω
$\left(R_{ss_{CT}}\right)_{2M}$	446.5 Ω	402.5 Ω	390.2 Ω
t_+	0.263	0.349	0.519
$(D)_{2M}$	3.43 × 10^{-13} m^2/s	3.28 × 10^{-13} m^2/s	3.09 × 10^{-13} m^2/s
δ	44.03 × 10^{-6} m	43.06 × 10^{-6} m	41.79 × 10^{-6} m
$(D)_{3M}$	2.70 × 10^{-13} m^2/s	2.65 × 10^{-13} m^2/s	2.39 × 10^{-13} m^2/s
a	5.54 × 10^{-13} m^2/s	5.02 × 10^{-13} m^2/s	5.17 × 10^{-13} m^2/s
b	0.000239 m^3/mol	0.000213 m^3/mol	0.000257 m^3/mol
C_s	71.6 mol.m^{-3}	185.8 mol.m^{-3}	598.1 mol.m^{-3}
j_d/j_s	2.293	1.809	1.352
j_d	1.146 mA.cm^{-2}	0.904 mA.cm^{-2}	0.676 mA.cm^{-2}

References

[1] B. Pant, Y. Ren and Y. Cao, *ACS Appl. Mater. Interfaces*, 2023, **15**, 59329–59336.

[2] G. Nagaraju, S. Tagliaferri, A. Panagiotopoulos, M. Och, R. Quintin-Baxendale and C. Mattevi, *J. Mater. Chem. A*, 2022, **10**, 15665–15676.